Nickel (II) Oxide Solubility and Phase Stability in High Temperature Aqueous Solutions

SE Ziemniak, and MA Goyette

Nickel(II) Oxide Solubility and Phase Stability

in High Temperature Aqueous Solutions

S. E. Ziemniak

M.A. Goyette

Lockheed Martin Corporation

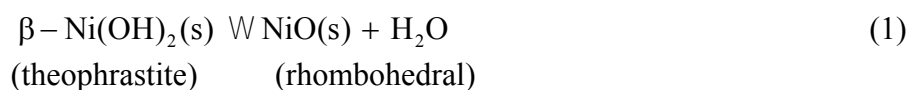P. O. Box 1072

Schenectady, New York 12301-1072

ABSTRACT

A platinum-lined, flowing autoclave facility was used to investigate the solubility behavior of nickel(II) oxide (NiO) in deoxygenated ammonium and sodium hydroxide solutions between 21 and 315°C. Solubilities were found to vary between 0.4 and 400 nmol kg^{-1}. The measured nickel ion solubilities were interpreted via a Ni(II) ion hydroxo-and ammino-complexing model and thermodynamic functions for these equilibria were obtained from a least-squares analysis of the data. Two solid phase transformations were observed: at temperatures below 149°C, the activity of Ni(II) ions in aqueous solution was controlled by a hydrous Ni(II) oxide (theophrastite) solid phase rather than anhydrous NiO (bunsenite); above 247°C, Ni(II) activities were controlled by cubic rather than rhombohedral bunsenite.
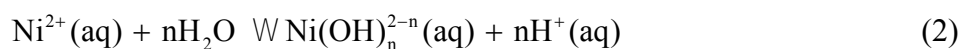
INTRODUCTION

The degradation of nickel base alloys used to contain hydrothermal solutions in the steam/water circuit of power plants can affect plant longevity and restrict power output. Although material corrosion rates are very low, the steady dissolution, transport and recrystallization of their protective oxide films may redistribute the corrosion products at selected locations throughout the plant. Such processes are driven by a combination of thermal gradients and alkalinity changes, as explained on the basis of nickel(II) oxide solubility studies conducted in mildly alkaline solutions. [1, 2] This work quantified the equilibria for the solid phase transformation reaction

$$\beta - Ni(OH)_2(s) \; \rightleftharpoons \; NiO(s) + H_2O \tag{1}$$
$$\text{(theophrastite)} \qquad \text{(rhombohedral)}$$

and the sequence of hydrolytic reactions

$$Ni^{2+}(aq) + nH_2O \; \rightleftharpoons \; Ni(OH)_n^{2-n}(aq) + nH^+(aq) \tag{2}$$

for n = 1-3 over the temperature range 25 to 300°C. In addition, a transformation of rhombohedral to cubic nickel(II) oxide is known to occur around 247°C.[3] This transformation is associated with disordering of the aligned magnetic moments of the nickel atoms (i.e., an antiferromagnetic-paramagnetic transformation).

Minimum solubilities of nickel(II) oxide, measured in hydrothermal solutions where the alkalinity was sufficient to stabilize the $Ni(OH)_2$(aq) hydroxocomplex, were found to be around 2 nmol kg^{-1} at 300°C.[1] A measurement uncertainty of ″ 40% is associated with these

measurements, as obtained from triplicate samples using the available analytical instrumentation (atomic absorption). Due in part to these large measurement uncertainties, a number of constraints were applied when thermodynamic properties of the nickel(II) ion hydrolysis products were extracted from the solubility database. As a result, the free energies of formation for $Ni(OH)^+$(aq) were rather poorly defined and in disagreement with independent free energy estimates of $Ni(OH)^+$(aq) formation near room temperature. [4]

Presently, advances in analytical sensitivity provided by flameless atomic absorption spectroscopy and inductively coupled plasma-mass spectroscopy allow the above uncertainties to be reduced. Therefore, our solubility studies of nickel(II) oxide[2] were extended to lower alkalinities using ammonia and sodium hydroxide at concentrations where the $Ni(OH)^+$(aq) and $Ni(OH)_2$(aq) hydroxocomplexes were expected to be stable.

Summarized herein are the results of a six-run test series that investigated the solubility behavior and phase stability of nickel(II) oxide (bunsenite) in aqueous ammonium and sodium hydroxide throughout the temperature range 21-315°C. The test methodology consisted of pumping various alkaline solutions of known composition through a bed of granular NiO and analyzing the emergent solutions for nickel. All test solutions were maintained oxygen-free by sparging with nitrogen. Equilibria for the following chemical reactions were described in thermodynamic terms: (a) $-Ni(OH)_2$ (theophrastite) or NiO (bunsenite) dissolution, (b) Ni(II) ion hydroxocomplex formation (hydrolysis) and (c) Ni(II) ion amminocomplex formation.

EXPERIMENTAL

Materials

To minimize generation of fine particulate material, which would interfere with the solubility measurements, a coarse, granular form of nickel oxide was prepared using certified nickel(ous) oxide, green, supplied by the Fisher Scientific Company (lot # 782699). The as-received powder was first compacted under 262 MPa pressure and attrited through a #8 mesh sieve (2.362 mm) onto a #20 mesh sieve (0.85 mm). The coarsened particles were then fired at 1200° C for 15 hours in an air furnace and quenched into liquid nitrogen. These sintering conditions proved to be insufficient, as many fines were observed during subsequent exposure to water washing. A second firing at 1450ºC for four hours, followed by quenching in liquid nitrogen, produced sufficiently dense particles that did not generate fines upon exposure to water.

The material produced in the above manner consisted of hard, irregular-shaped, olive-green particles with dimensions 0.85-2.4 mm. Density determinations using a mercury pycnometer gave a value of 5.447 g cm^{-3} (80% of theoretical). Powder X-ray diffraction analyses, performed using copper K$_\alpha$ radiation, confirmed the absence of impurity phases (<0.2%, detectability limit).

Two polymorphs of nickel(II) oxide are known: rhombohedral and cubic (bunsenite), i.e., Powder Diffraction File Nos. 44-1159 and 47-1049, respectively.[5] Although all of the lower angle diffractions were consistent with cubic NiO, examination of the higher angle peaks (2θ>100°) revealed peak splittings characteristic of a rhombohedral phase, see Fig. 1. The calculated lattice parameters were a = 2.9552(1) and c = 7.2275(3) Å. These values are in exact agreement with those in the PDF database. [5]

Deionized, deoxygenated water (obtained from charcoal and mixed-bed ion exchange resin columns) was used throughout the experimental program. This water had a resistivity >10 Mohm-cm and contained <0.1 mg L^{-1} silica. Trace contaminant levels of iron (2 nmol kg^{-1}) and nickel (3-6 nmol kg^{-1}) were present in the water during the first phase of solubility testing ($\leq$149°C), which were reduced to <0.8 nmol kg^{-1} during the final test phase. Commercial-grade nitrogen gas was used to sparge dissolved oxygen to values <0.005 mg L^{-1}. Test solutions were prepared volumetrically in the feed tanks using ultrapure ammonium hydroxide, or in some cases, reagent grade sodium hydroxide (Labchem, 50 wgt/vol %). .

Apparatus

The solubility measurements were made using the flowing autoclave arrangement shown in Fig. 2. The feed tanks, pump, filter holder and tubing between the feed tanks and first autoclave were stainless steel. The two test autoclaves were stainless steel with platinum liners. The tubing, cooler and valves (which comprised the sampling station) were stainless steel, the tubing and cooler having platinum linings. The feed tanks, each having a 115 liter capacity, were filled with deoxygenated, deionized water. Midway through the test program the feed tanks were teflon-lined and equipped with supplemental ion exchange capability to reduce contaminant input levels of nickel to <0.8 nmol kg^{-1}. Additions of solutions containing reagent grade chemicals were made to obtain the desired feedwater compositions. These compositions are listed in Table I.

Nitrogen gas was bubbled through the feed solution and one atmosphere of this gas was maintained over the feed solution during all tests. The nitrogen concentration in the feedwater was calculated to be 1115 F mol kg^{-1} based on pressure in the feed tank and Henry's law coefficient for the solubility of nitrogen in water.[6]

A Milton Roy piston-type pump supplied feedwater to the high-pressure system. A flow rate of 6.0 " .5 cm^3 min^{-1} (at room temperature) was maintained. From the pump, the (ambient temperature) feedwater passed through a high-pressure filter holder containing a 0.2 μm Uni-Pore⌡ polycarbonate filter membrane. After the filter, the feed solution entered two platinum-lined autoclaves connected in series. Each autoclave had an internal volume of - 100 cm^3 (2.5 cm diam. x 20 cm length). The first autoclave was empty and acted as a solution preheater, whereas the second autoclave contained 329 grams of nickel(II) oxide. The coarsened particles were confined to the test autoclave by means of a fine platinum screen at the inlet and a sintered, micrometallic, disc-type filter at the outlet. To increase the hot filtering capacity of the frit, it was compressed from an initial thickness of 2.45 to 1.65 mm.

The average contact time between the feed solution and the bed was 4.6 to 6.7 minutes, depending on the temperature. Based on experience gained during our previous NiO solubility study, [2] these contact times were sufficient to achieve saturation solubility levels. By way of comparison, previously unreported nickel(II) oxide solubility measurements, obtained in ammonium hydroxide during our 1985 test program, [2] are included in Table II. No differences are apparent.

After leaving the second autoclave, the test solution flowed immediately through a stainless steel cross, one leg of which was dead-ended and contained a platinum-sheathed thermocouple to monitor temperature of the exiting solution. The main leg directed flow into the sampling line, while the remaining leg provided a secondary path through which flow could be diverted in case

the sampling line became plugged. This leg was also connected to a pressure gauge which monitored system pressure.

The sampling system consisted of a water-jacketed cooler and a pressure-regulating valve, located immediately upstream of the sample collection point. For safety purposes, a second valve (which always remained open) was installed between the cooler and pressure-regulating valve. All tubing between the two autoclaves and between the outlet of the second autoclave and sample collection point, including the cooler, were high-pressure Alloy 600 tubing lined with platinum. Both valves in the sampling system were stainless steel and had titanium internals. During normal operation, the system pressure was maintained in the range 13.1-14.1 MPa.

Heat was supplied to the autoclaves by a Chromalox electrical heating element jacket, the temperature being controlled by a Modicon PID programmable logic controller (PLC). System temperatures were monitored with iron-constantan (J Type) thermocouples at three locations: (1) outer surfaces of the first and second autoclaves (4 in parallel per autoclave, read as an average), (2) tubing at entrance and outlet of the second autoclave (2), and (3) in the flow stream at the second autoclave outlet. The thermocouples had been purchased with a stated ⋃pecial error limit⋃ of ˮ 1.1°C; their outputs were also displayed on the PLC.

Operational and Analytical Procedures

In anticipation of a solid-phase transformation reaction, demonstrated to occur in previous solubility testing of nickel(II) oxide, [2] the test program was conducted in two stages: a low temperature portion (21-149°C), followed by a high temperature portion (149-315°C). All low

temperature runs were completed prior to the high temperature runs to eliminate system

hysteresis effects due to sluggish hydration/dehydration effects.

Prior to the start of each test run, one of the feed tanks was prepared by rinsing, flushing and

filling with demineralized water. After chemical addition, the tank was sparged with nitrogen

gas to facilitate mixing and to minimize oxygen. A one-atmosphere blanket of nitrogen gas was

placed over the feed water upon completion of the sparging operation. The NiO bed was then

flushed for a minimum of three days, using a system flow rate of six cm^3 min^{-1}. The flushing

period insured adequate time for equilibration with each test chemistry. The sampling sequence,

during which six samples were collected in autosampler vials, was then initiated. After

sampling, the PLC was set to establish a new temperature. Although 120 to 150 minutes were

required to establish the new temperature, the system was allowed to stabilize at the new

temperature for at least one day before the sampling procedure was repeated.

In a similar manner, each high temperature sequence was initiated after system operation at

260°C for at least 3 days. The sampling sequence was conducted in an increasing/decreasing/

increasing mode so that the 163 to 316°C interval was completed in increments of 14°C.

Feed tank and system effluent samples were collected during each run and analyzed for pH,

conductivity and oxygen. Ammonia was determined by ion chromatography, while sodium

hydroxide was determined by acid-base titration using standardized hydrochloric acid solutions.

GFAA

All liquid samples collected during the low temperature test stage were analyzed for nickel by flameless atomic absorption techniques. A Perkin-Elmer Model 5000 Zeeman Atomic Absorption Spectrophotometer, equipped with a graphite furnace, was used. A set of standard solutions (0.1 M nitric acid containing known amounts of nickel) was analyzed with each group of samples. The normal analytical procedure was to collect approximately a 2 cm^3 sample aliquot in an acid-leached, polystyrene autosampler vial to which 25 µL of concentrated, high purity nitric acid had been added. Samples containing <17 nmol kg^{-1} Ni were pre-concentrated using multiple delivery and drying steps prior to performing the atomization step. Analytical accuracy is expected to decrease with concentration: " 10% for $\geq$ 17 nmol kg^{-1} to " 30% at 3 nmol kg^{-1}.
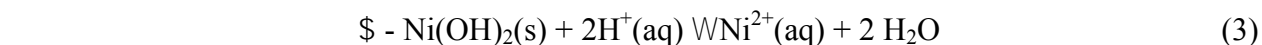
ICPMS

Due to the lower nickel solubilities encountered during some of the high temperature runs, larger volume samples (~ 30 cm^3) were collected in acid-leached Nalgene bottles. The samples were acidified to 0.5% or 1.0% nitric acid at least one day prior to analysis. Additional samples were obtained from the teflon-lined feed tanks to determine background levels of nickel in the feedwater. An HP4500 Series 300 Inductively Coupled Plasma Mass Spectrometer manufactured by Hewlett-Packard was used for these analyses. Analytical accuracy is expected to be better than " 20% above 0.2 nmol kg^{-1}.
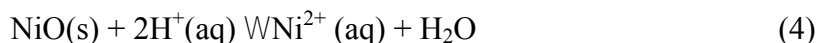
RESULTS

Solubility Measurements/Reactions

Results from the experimental program, in terms of measured nickel solubilities as a function of

temperature, are presented in Tables II and III. The elemental nickel concentrations represent

averages of six samples and are given in units of nmol kg^{-1} (10^{-9} moles of nickel per kilogram of

water). The small amounts of material lost in the sampling line have been neglected. The

temperature value listed for a particular sample was the downstream thermocouple reading after

sampling was completed. Total measured nickel solubilities ranged between 0.4 and 400 nmol
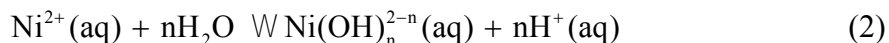
kg^{-1}.

Given the hydrothermal environments in which nickel(II) oxide was exposed, two dissolution

reactions and two sequences of Ni(II) hydrolysis and amminocomplexing reactions are possible:

$$\$ - Ni(OH)_2(s) + 2H^+(aq) \rightleftharpoons Ni^{2+}(aq) + 2\ H_2O \tag{3}$$

or

$$NiO(s) + 2H^+(aq) \rightleftharpoons Ni^{2+}\ (aq) + H_2O \tag{4}$$

and

$$Ni^{2+}(aq) + nH_2O \ \rightleftharpoons Ni(OH)_n^{2-n}(aq) + nH^+(aq) \tag{2}$$

$$Ni(OH)_n^{2-n}(aq) + NH_3(aq) \rightleftharpoons Ni(OH)_n(NH_3)^{2-n}(aq) \tag{5}$$

where n = 0, 1, 2 and 3.

By expressing the concentration of each possible Ni(II) ion complex in terms of an equilibrium

constant and calculable H$^+$ ion and undissociated NH$_3$ concentrations, the measured Ni(II) ion

solubilities were separated into contributions from each of the individual complexes. The total

molality of nickel in solution (i.e., saturation solubility limit) was then calculable by summation

over all mononuclear Ni(II) ion species present.

Post-operational Material Characterization

Inspection of the nickel oxide packed column at the conclusion of the test program revealed no visible changes, i.e., no settling or degradation into fines. High magnification views, obtained by scanning electron microscopy (3-10, 000 X), confirmed the absence of bulk surface changes (see Fig. 3). These images also demonstrate the effectiveness of the sintering process in bonding individual oxide grains having ultimate sizes around 3-4 Fm. Powder XRD analysis performed after crushing the coarse particles confirmed the presence of a single-phase rhombohedral lattice whose parameters were unchanged from the original material.

Examination of individual NiO crystallites by X-ray photoelectron spectroscopy (XPS) revealed that a submicroscopic layer of hydrous nickel(II) oxide was present on the surface of material removed from the solubility apparatus. Verifying the presence of $Ni(OH)_2$ via a chemical shift in electron binding energies in the $Ni(2p^{3/2})$ core region (854.0 eV for NiO vs. 855.9 eV for $Ni(OH)_2$) is complicated by interference from a shoulder on the high binding energy side of the NiO spectrum.[7] However, the presence of $Ni(OH)_2$ was readily confirmed by investigating the O(1s) electron binding energies (see Fig. 4). These energies are 529.6 and 531.4 eV for NiO and $Ni(OH)_2$, [7] respectively.

The intensity of the 531.4 eV (hydroxide) peak relative to the 529.6 eV (oxide) peak is extremely sensitive to the amount of argon ion bombardment. Normally, ion milling can be used for depth profiling. However, when a $Ni(OH)_2$ standard was subjected to sputtering argon ion bombardment, significant $Ni(OH)_2$ conversion to NiO was observed for milling times as short as 10 s. [8] This behavior is consistent with the apparent presence of NiO in Fig. 4b; see O(1s) peak at 529.6 eV in posttest material cleaned by sputtering for 12 s to remove adsorbed carbonaceous

contaminants. Thus, it was not possible to determine the thickness of the Ni(OH)$_2$ layer by XPS, since the sputter-induced disappearance of the 531.4 eV peak could be associated with dehydration to NiO as well as the desired removal of Ni(OH)$_2$.

pH Determination

Evaluation of the experimental solubilities of Tables II and III in terms of concentrations of the possible hydrolyzed/complexed Ni(II) species present required that the pH (hydronium ion concentration) be known at the existing solution conditions. This quantity depended on the molality of the alkaline reagents dissolved in solution (i.e., ammonia or sodium hydroxide), as well as their ionization constants and that of H$_2$O. The latter parameters, which are functions of solution temperature, are defined below in terms of thermodynamic activities ( ) and tabulated in Table IV.

$$K_w = (\text{H}^+)\,(\text{OH}^-) \tag{6}$$

$$K_B = (\text{NH}_4^+)\,(\text{OH}^-)\,/\,(\text{NH}_3) \tag{7}$$

$$\text{with} \qquad \log K = b_1\,/T + b_2 + b_3 \ln T + b_4 T + b_5\,/T^2 \tag{8}$$

Both K_w and K_B were pressure-corrected (to 13.1 MPa), as well as ionic strength-corrected, using the correlations. [9, 10]

Equilibrium constants for Eqs. (2) - (5) were corrected for small deviations from ideal solution behavior by distinguishing between ionic concentration (i.e., molality) and thermodynamic activity

$$\left(a_i\right) = \gamma_i\left[C_i\right] \tag{9}$$

where (a_i) is the thermodynamic activity, γ_i the ionic activity coefficient and [C_i] is the ionic

concentration. Generally, it was assumed that ionic activity was related to ionic strength by an

extended Debye-Hdckel expression[11]

$$\log \gamma_i \;=\; -SZ_i^2 \sqrt{I}/(1 + 1.5\sqrt{I}) \tag{10}$$

where S is the temperature-dependent,[12] limiting Debye-Hdckel slope (0.51 at 298 K), Z_i is the

ionic charge number, and I is the ionic strength (= ($\mathbf{2}$) $\Sigma C_i Z_i^2$).

An overall ion electroneutrality balance was finally applied to determine [H^+] for each data point.

In ammonium hydroxide solutions, the balance is:

$$\sum_{n=0}^{3} (2-n)[Ni(OH)_n^{(2-n)+}] \;+\; \sum_{m=0}^{3} (2-m)[Ni(OH)_m(NH_3)^{(2-m)+}] \tag{11}$$
$$+ \; [NH_4^+] \;+\; [H^+] \;=\; [OH^-]$$

The relatively low ammonia concentrations, together with existing information on multiple

ammonia complexing equilibria,[13] indicate that multiple ammonia complex concentrations are

expected to be low and have a negligible impact on pH. Hence the added complexity introduced

by their inclusion in the neutrality balance is not justified.

Since all terms were expressible in terms of temperature and total dissolved ammonia

concentrations, Eq. (11) was reduced to an algebraic equation in terms of the remaining

unknown, [H^+]. To determine how a given scheme of Ni(II) complexes in solution could fit the

results, a set of thermodynamic constants was substituted into the neutrality balance, and [H^+]

concentrations were calculated by a Newton-Raphson iteration procedure. These [H^+] values

were then used to compute all the soluble nickel species which, after being summed, could be compared with the measured Ni solubilities. The differences were then minimized via a generalized, non-linear, least-squares curve-fitting routine based on Marquardt's algorithm.[14]

When the solubility data were analyzed, the importance of relative errors (i.e., percentage errors), rather than absolute errors, was accounted for by minimizing differences between the logarithms of the experimental and the predicted solubilities. The thermodynamic functions obtained were then resubstituted into the neutrality balance, and the two step process was repeated. Convergence, i.e., the condition when the calculated thermodynamic functions ceased to change, was attained in a few cycles because the dissolved metal ion concentrations were very low and had only a minor influence on changes in solution pH.

Thermodynamic Analysis

The thermodynamic relationships

$$-RT \ln K = \Delta G^o = \Delta H^o - T\Delta S^o \tag{12}$$

were introduced at this point to permit calculation of all Ni(II) ion complex concentrations as functions of temperature using two parameters (ΔH^o and ΔS^o). In two cases, a three-parameter model was used to describe $\Delta G^o(T)$. This approximation assumes that the difference in heat capacities between reactants and products for each reaction is a constant (C). Integration of the applicable thermodynamic relationship gives

$$\Delta G^o(T) = A - BT - CT \ln T \tag{13}$$

where the constants A, B and C have the thermodynamic significance: $A = \Delta H^o(298) - 298\Delta C_p^o$; $B = \Delta S^o(298) - (1 + \ln 298)\Delta C_p^o$; and $C = \Delta C_p^o$. Normally, inclusion of the heat capacity term in

Eq. (13) is unwarranted. It is, in fact, possible to minimize curvature in hydrolytic $\Delta G^o(T)$ correlations by rewriting the reaction, using H^+ or OH^- ions as needed, to balance like charges on the reactant side with those on the product side. By this 'isocoulombic' principle,[15] it is seen that only the n = 3 form of Eq. (2) is <u>not</u> in the form which minimizes heat capacity effects. Therefore, a heat capacity effect on the order of -224 J mol^{-1} K^{-1}, *i.e.*, that equivalent to $\Delta C_p{}^o$ for the water ionization reaction, is expected for the Eq. (2) equilibrium which creates the Ni(OH)$_3{}^-$ species. On the other hand, the equilibrium for Eq. (4) is complicated by the existence of a bunsenite heat capacity anomaly at 247°C, which was addressed by allowing curvature in the $\Delta G^o(T)$ correlation for Eq. (4) at temperatures above 246°C via Eq. (13).

The effects of two solid phase transformations were accounted for by: (1) assuming the presence of a Ni(OH)$_2$/NiO phase boundary at 155°C, fitting thermodynamic properties for both solids, and then recalculating the phase boundary provided by the least-squares analysis, and (2) fitting a three parameter $\mathit{)}\,G^o(T)$ model for the Eq. (4) dissolution reaction equilibrium above 247°C to allow for the rhombohedral to cubic transformation of NiO. [3]

Results of the above data fitting procedure are shown in Figs. 5 - 7. In these plots the theophrastite dissolution reaction equilibrium, i.e., Eq. (3), as well as the ammonia complexing equilibria, and all but one of the Ni(II) ion hydrolytic equilibria were fitted using Eq. (13) with C = 0. An initial, unconstrained fit of C for the Eq. (4) equilibrium resulted in an unrealistically high (and imprecise) value, presumably reflecting the scatter in our solubility data. Upon examining the bunsenite heat capacity measurements of Hemingway, [3] we estimate that a heat capacity change on the order of 40 J mol^{-1} K^{-1} may be contributed by the heat capacity anomaly. Therefore, the undesirable behavior was eliminated by fitting the equilibrium for Eq. (4) in two

segments: below 247°C, C = 0; above 247°C, C = 40 J mol^{-1} K^{-1}. In this manner, statistically

significant fits were obtained for the thermodynamic functions of the unhydrolyzed Ni^{2+}(aq) ion

and four of its hydrolytic products: Ni(OH)$^{+}$, Ni(OH)$_2$(aq), Ni(OH)(NH$_3$)$^{+}$ and

Ni(OH)$_2$(NH$_3$)(aq).

Table V presents the fitted thermochemical parameters for the Ni(II) oxide dissolution reactions

and the applicable hydrolysis and complexing reactions. These fits resulted in an overall

standard deviation between measured and fitted nickel solubilities of $"$ 24% for a database

consisting of 147 entries. This level of uncertainty is consistent with the improved analytical

sensitivities available at sub-nanomolal concentrations.

DISCUSSION OF RESULTS

A. Extraction of Thermodynamic Properties for Ni^{2+}(aq)

The present Ni(II) ion solubility database was interpreted by recognizing equilibria for the

dissolution of three solid-phases: hydrous nickel(II) oxide (theophrastite), rhombohedral

nickel(II) oxide and cubic nickel(II) oxide. The standard free energy changes fitted for the first

two reactions: -67.41 $"$ 0.47 kJ mol^{-1} and -70.32 $"$ 0.98 kJ mol^{-1}, respectively (see Table V),

agree well with independent literature results. For example, recent solubility measurements of

theophrastite at room temperature[16] give ΔG^o (298) = -67.91 $"$ 0.59 kJ mol^{-1} for Eq. (3), while

refined thermodynamic properties for Ni^{2+}(aq),[17] bunsenite[3] and water[13] give ΔG^o (298) =

-69.94 kJ mol^{-1} for Eq. (4).

Temperature dependencies for the Eqs. (3, 4) equilibria are plotted in Fig. 8. A **⊔**iterature**⊔**

estimate for the theophrastite dissolution equilibrium, Eq. (3), was obtained by employing a

$\Delta H_f^\circ(298)$ value for β-Ni(OH)$_2$ extracted from a Fisher-Zen analysis[18] of data for the β-Ni(OH)$_2$/NiO transformation. The latter analysis gave ΔH_f°(theophrastite) = ΔH_f°(bunsenite) - 291.83 kJ mol^{-1}.[19] This result provides

$$\Delta G^o \ (T), \text{ J mol}^{-1} = -94130 + 87.94T \tag{14}$$

for Eq. (3). Independently-estimated free energy changes for the bunsenite dissolution reaction, Eq. (4), based on available ΔG_f^o (298), S° (298) and C_p^o (298) values for NiO[3], Ni^{2+}(aq)[17, 20] and water[13] give

$$\Delta G^o(T), \text{ J mol}^{-1} = -96302 + 15.26T + 12.84T \ ln \ T \tag{15}$$

Eq. (15) is expected to become less accurate above 520 K due to its inability to account for the heat capacity anomaly associated with the transformation of rhombohedral to cubic NiO. Despite this shortcoming, Eqs. (14, 15) are seen to agree with the present experimental results to within 3 kJ mol^{-1} over the temperature range of the study, see Fig. 8.

It is of interest to note that the $\Delta G^o(T)$ correlation for Eq. (4) based on previous solubility measurements [1] deviate from the literature predictions by more than 6 kJ mol^{-1} at the upper temperature limit due to a greater sensitivity to temperature changes (see Fig. 8). This behavior is believed to be an artifact caused by too large a ΔC_p^o value for Eq. (4), i.e., -77.9[1] vs. -12.8 J mol^{-1} K^{-1}.

A refined set of thermodynamic properties for Ni^{2+}(aq) may be extracted from the fitted equilibrium for the rhombohedral NiO dissolution reaction given in Table V by assuming that most of the discrepancy between prediction and measurement lies in the assumed properties for
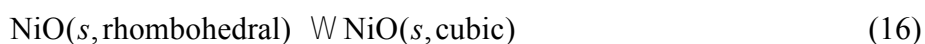
Ni^{2+}(aq), whose stated uncertainty is $\pm$ 2 kJ mol^{-1}.[4] Therefore, combining the more precise

solubility-based equilibrium for Eq. (4) with the properties of NiO and H_2O gives ΔG_f^{o}(298) =

-44.28 kJ mol^{-1}, ΔH_f^{o}(298) = -52.42 kJ mol^{-1} and $S°$(298) = -172.5 J mol^{-1} K^{-1} for Ni^{2+}(aq).

In a similar manner, a refined set of thermodynamic properties for β-Ni(OH)$_2$ may be extracted

from the fitted equilibrium for the theophrastite dissolution reaction (Table V) using the above-

refined properties for Ni^{2+}(aq): ΔG_f^{o}(298) = -451.15 kJ mol^{-1}, ΔH_f^{o}(298) = -534.98 kJ mol^{-1} and

$S°$(298) = 84.5 J mol^{-1} K^{-1}.

B.   Nickel(II) Oxide Solid Phase Transformations

Estimation of the dehydration temperature for Eq. (1), based on equality of the fitted free energy

changes for Eqs. (3) and (4) provided in Table V, yields a threshold temperature of 149°C. An

independent estimate, derived from literature-based predictions of the equilibria for Eqs. (3, 4) in

the previous section, i.e., Eqs. (14, 15), is calculated to be 154°C. The good agreement between

measurement and prediction is further supported by recent observations regarding the stable

oxide layer formed on corroding nickel surfaces exposed in non-deaerated, hydrothermal

systems: a transformation from β-Ni(OH)$_2$ to NiO occurred around 160°C.[21] Therefore, the

results from our previous nickel(II) oxide solubility study, which indicated a transformation at

195°C,[2] were probably biased by sluggish dehydration kinetics.

The transformation from rhombohedral to cubic nickel(II) oxide

$$NiO(s, \text{rhombohedral}) \rightleftharpoons NiO(s, \text{cubic}) \qquad (16)$$

occurs nearly simultaneously with a loss of magnetic ordering. Unlike the C_p anomaly observed

in other antiferromagnetic oxides (i.e., a rapid decrease from a peak value), the heat capacity of
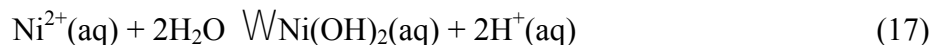
bunsenite decreases slowly with temperature beyond 246°C, and continues until 434°C, when a minimum is reached and further temperature increases again lead to increases in heat capacity.[3] Therefore, an <u>increase</u> in $)C_p$ for the Eq. (4) dissolution reaction equilibrium is expected at temperatures above 247°C. The impact of this thermal anomaly on the calculated free energy changes was modeled by constraining $C = 40$ J mol^{-1} K^{-1} via Eq. (13) for temperatures above 247°C. Allowing for the limitations of Eq. (13), the qualitative agreement between fit and expectation is considered adequate.

C.   <u>Nickel(II) Ion Hydrolysis</u>

Free energy changes for the first two hydrolysis reactions are plotted in Fig. 9. The standard free energy change for the first hydrolysis reaction was found to be 53.89 ¨ 0.65 kJ mol^{-1}. This result compares favorably with a literature value of 55.14 ¨ 0.17 kJ mol^{-1} [4, 13] and represents an improvement over the result obtained from a previous high temperature solubility study of NiO, 68.6 ¨ 9.4 kJ mol^{-1},[1] which was considered inconclusive.

The present results are believed to be the first reliable determination of the equilibrium for the n = 1 form of Eq. (2) at high temperatures. Agreement with the Refs. (4, 13) results is considered to be excellent, given the limited temperature range (15-42°C) of the previous study. On the other hand, the previous Ref. 1 results straddle the present results by ¨ 7 kJ mol^{-1} at temperatures between 125 and 275°C. The larger deviations at temperatures above 260°C appear to be a compensation for the inappropriate $)C_p^o$ value used by Ref. 1 to fit free energy changes for the bunsenite dissolution reaction, Eq. (4).

Gibbs energy changes fitted to the two step hydrolysis reaction

$$Ni^{2+}(aq) + 2H_2O \rightleftharpoons Ni(OH)_2(aq) + 2H^+(aq) \qquad (17)$$

per Table V are also plotted in Fig. 9. The standard Gibbs energy change for Eq. (17) is 129.41

$\pm$ 3.16 kJ mol^{-1}. The higher uncertainty in $\Delta G°(298)$ for Eq. (17) is caused by extrapolation of

very low fitted concentrations of the Ni(OH)$_2$(aq) species, having a normal sensitivity to

temperature changes, to room temperature. For example, the expected concentration of

Ni(OH)$_2$(aq) resulting from theophrastite dissolution at 25°C is 0.01 nmol kg^{-1}. Concentrations

of the Ni(OH)$^+$(aq) and Ni(OH)$_2$(aq) species in Run 5 do not become equivalent (i.e., 0.17 nmol
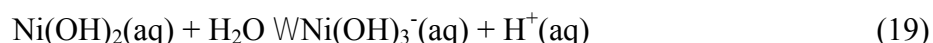
kg^{-1}) until the temperature reaches 185°C.

It is noted that free energy changes for Eq. (17) were determined previously [1, 2] by subtracting

free energy changes for Eq. (4) from those determined for

$$NiO(s) + H_2O \rightleftharpoons Ni(OH)_2(aq) \qquad (18)$$

Due to the apparent bias in the Ref. 1 fit for Eq. (4) and the lack of appropriate data in Ref. 2 to

determine $\Delta G°(T)$ for Eq. (4), the Table V parameters for Eq. (4) were combined with the results

of Refs. 1 and 2 for Eq. (18) to provide a mutually-consistent basis upon which to compare

$\Delta G°(T)$ estimates for the two step hydrolysis reaction. Fig. 9 shows that the revised $\Delta G°(T)$

estimates of Ref. 2 are about 5-6 kJ mol^{-1} lower than those of the revised Ref. 1 estimates. This

difference is probably caused by underestimation of phosphatocomplexing in the Ref. 2 study.

However, the present results are more than 7 kJ mol^{-1} greater than the revised Ref. 1 estimates. This difference is indicative of the significantly lower minimum Ni(II) ion solubilities measured at elevated temperatures: 0.5 nmol kg^{-1} (Runs 5, 6) versus 3 nmol kg^{-1} (Ref. 1) at 260°C.

Previous NiO solubility measurements at elevated temperatures had reported that the Ni(II) ion third stepwise hydrolysis reaction
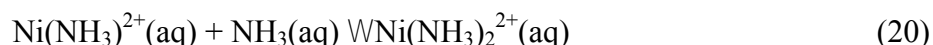
$$Ni(OH)_2(aq) + H_2O \rightleftharpoons Ni(OH)_3^-(aq) + H^+(aq) \tag{19}$$

occurred when sodium hydroxide concentrations exceeded 3 mmol kg^{-1}, i.e., pH (at 25°C) >11.4. [1,2] In these solutions bunsenite solubilities increased with sodium hydroxide concentration as well as temperature. Although Runs 5 and 6 indicated that bunsenite solubilities had indeed reached minimum levels with respect to alkalinity changes, and had begun to increase with temperature, solubility increases with respect to alkalinity increases were not observed, compare Figs. 6 and 7. Such behavior indicates that Ni(OH)$_2$(aq), rather than Ni(OH)$_3^-$(aq), was controlling NiO solubility at these hydroxyl ion concentrations.

Attempts to include the Eq. (19) equilibrium in regression analyses of the present database were unsuccessful, as they resulted in no significant reduction in least-squares residuals.

D.   Nickel(II) Ion Amminocomplexing

Given the known complexing ability of the ammonia molecule for the divalent nickel cation, [22] formation of Ni(NH$_3$)$^{2+}$(aq) via the n = 0 form of Eq. (5) is expected to occur at free ammonia concentrations above 2 mmol kg^{-1}. Incorporation of a second ammonia ligand via

$$Ni(NH_3)^{2+}(aq) + NH_3(aq) \rightleftharpoons Ni(NH_3)_2^{2+}(aq) \tag{20}$$

occurs at free ammonia concentrations above 6.5 mmol kg^{-1}. Since free ammonia concentrations were around 0.6 and 6 mmol kg^{-1} in Runs 2 and 3, respectively, it was prudent to fit up to two ammonia ligands in the sequence of Ni(II) ion hydrolysis products to form mixed amminohydroxocomplexes.

The enhancement of nickel(II) oxide solubility by formation of ammonia complexes is illustrated by comparing the results of Run 3 (Fig. 5, pH 10.4 ammonium hydroxide) and Run 4 (Fig. 4, pH 10.3 sodium hydroxide). Due to the characteristic hydrolysis behavior of Ni(II), the dominant soluble Ni(II) ion species in the low temperature portions of the figures existed as Ni(OH)$^+$(aq). Therefore, the higher Ni(II) ion solubilities in Run 3 at lower temperatures were fitted by allowing formation of the Ni(OH)(NH$_3$)$^+$(aq) amminohydroxocomplex. The standard free energy change fitted for Eq. (5) (n = 1), i.e., -17.34 $^"$ 0.61 kJ mol^{-1}, compares favorably with that for the n = 0 equilibrium, i.e., - 15.48 kJ mol^{-1}, indicating that hydrolysis does not significantly affect amminocomplexing. It is noted that Ni^{2+}(aq) ion concentrations tended to be insignificant when the higher levels of ammonia were tested. This behavior allowed formation of the Ni(NH$_3$)$^{2+}$(aq) and Ni(NH$_3$)$_2$$^{2+}$(aq) amminocomplexes to be constrained to literature results [22] without loss of generality.

In the high temperature region of Run 3, where hydrolysis provided significant concentrations of Ni(OH)$_2$(aq), NiO solubilities tended to become relatively insensitive to temperature changes. This behavior contrasted with Run 4, where, at nearly the same pH level, NiO solubilities decreased significantly with temperature. Such behavior indicates the presence of an additional amminocomplex, namely Ni(OH)$_2$(NH$_3$)(aq). Although the standard free energy change for the
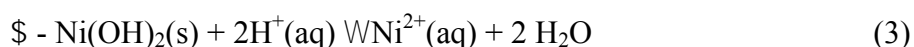
n = 2 form of Eq. (5) (-15.72 " 5.28 kJ mol^{-1}) was found to be nearly the same as that for the n =

0 and 1 forms, the entropy increase associated with this equilibrium allows Ni(OH)$_2$(NH$_3$)(aq) to

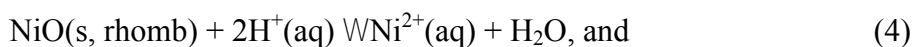remain important at high temperatures (see Fig. 10).

SUMMARY/CONCLUSIONS

The solubility behavior of nickel(II) oxide (NiO) was investigated in a platinum-lined, flowing

autoclave system over the temperature range 21 to 315°C using ammonia concentrations in the

range 0.06 to 6 mmol kg^{-1}. To separate the effects of pH and ammonia concentration, additional

runs were included using sodium hydroxide. Based on the accumulated database and the

subsequent thermodynamic analyses afforded the data , it is concluded that:

1.   Depending on temperature, nickel(II) ion solubilities are controlled by one of three
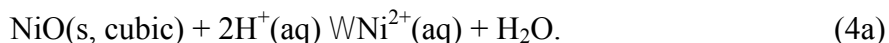
nickel(II) oxide dissolution reactions:

(a) Below 149°C a hydrous nickel oxide phase ($-Ni(OH)$_2$, theophrastite) controls the

dissolution reaction equilibrium via

$$\$ - Ni(OH)_2(s) + 2H^+(aq) \lor Ni^{2+}(aq) + 2\ H_2O \tag{3}$$

(b) Above 149°C, but below 247°C, anhydrous rhombohedral nickel oxide (NiO,

bunsenite) controls the dissolution reaction equilibrium via

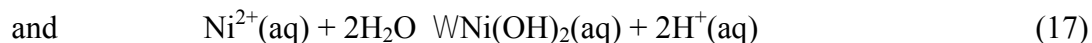$$NiO(s, rhomb) + 2H^+(aq) \lor Ni^{2+}(aq) + H_2O, and \tag{4}$$

(c) Above 247°C cubic nickel(II) oxide controls the dissolution reaction equilibrium via

$$NiO(s, cubic) + 2H^+(aq) \lor Ni^{2+}(aq) + H_2O. \tag{4a}$$

Non-linear, least-squares regression analyses of the solubility database allowed free energy

changes for all three reactions to be determined with accuracies of " 0.8 kJ mol^{-1} throughout their

applicable temperature ranges. The standard free energy changes (i.e., values at room temperature) are found to be in excellent agreement with recent literature results. Inclusion of the rhombohedral-to-cubic transformation of NiO was found necessary to account for the heat capacity anomaly caused by disordering of magnetic spins on nickel atoms in the NiO lattice.
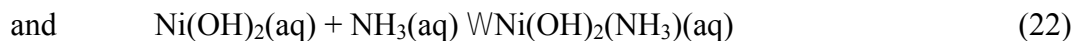
2.   Equilibria for the formation of two nickel(II) ion hydrolysis products were found to be significant, and were characterized by the following reactions:

$$Ni^{2+}(aq) + H_2O \rightleftharpoons Ni(OH)^+(aq) + H^+(aq) \tag{2}$$

$$\text{and} \qquad Ni^{2+}(aq) + 2H_2O \rightleftharpoons Ni(OH)_2(aq) + 2H^+(aq) \tag{17}$$

Free energy changes for the first and second reactions were determined with accuracies of $\pm$ 0.8 and $\pm$ 3.1 kJ mol^{-1}, respectively, throughout the temperature range 21 to 315°C. Standard free energy changes for the first hydrolysis reaction demonstrated excellent agreement with the room temperature literature. However, the much lower minimum solubilities of β-Ni(OH)$_2$ at room temperature measured in the present program provided standard free energy changes for the second hydrolysis reaction that were more than 20 kJ mol^{-1} greater than reported in the literature. Similar differences were also obtained at elevated temperatures: minimum solubility of NiO at 300°C (0.5 nmol kg^{-1}) was lower than reported in the literature (1.7 nmol kg^{-1}).[1]

3.   No evidence was found to support inclusion of the third hydrolytic species, Ni(OH)$_3^-$(aq), despite testing at sodium hydroxide concentrations up to 4 millimolal, i.e., pH = 11.5. A summary of extracted thermochemical properties for known species in the NiO-H$_2$O binary is given in Table VI.

4.   The equilibria for two ammonia complexing reactions were found to enhance nickel(II)

ion solubilities at intermediate ammonia levels:

$$Ni(OH)^+(aq) + NH_3(aq) \rightleftharpoons Ni(OH)(NH_3)^+(aq) \qquad (21)$$

$$\text{and} \qquad Ni(OH)_2(aq) + NH_3(aq) \rightleftharpoons Ni(OH)_2(NH_3)(aq) \qquad (22)$$

The first is a low temperature species and constitutes 35% of the room temperature solubility of

β-$Ni(OH)_2$ in pH 10 NH_4OH; the second is a high temperature species and contributes about 5%

to the solubility of NiO at 260°C in the same NH_4OH solution. At pH 10.3 and 260°C, the

$Ni(OH)_2(NH_3)(aq)$ species represents 25% of the soluble Ni(II) ions.

REFERENCES

1.	P. R. Tremaine and J. C. LeBlanc, J. Chem. Thermodyn. **12**, 521 (1980)

2.	S. E. Ziemniak, M. E. Jones and K. E. S. Combs, J. Solution Chem. **18**, 1133 (1989)

3.	B. S. Hemingway, Amer. Mineral. **75**, 781 (1990)

4.	D. D. Perrin, J. Chem. Soc. 3644 (1964)

5.	JCPDS Powder Diffraction File, International Centre for Diffraction Data, Swarthmore, PA (1999), Sets 1-49

6.	D. M. Alexander, D. J. T. Hill and L. R. White, Aust. J. Chem. **24**, 1143 (1971)

7.	N. S. McIntyre, T. E. Rummery, M. G. Cook and D. Owen, J. Electrochem. Soc. **123**, 1164 (1976)

8.	N. S. McIntyre and D. G. Zetaruk, J. Vac. Sci. Technol. **14**, 181 (1977)

9.	F. H. Sweeton, R. E. Mesmer, and C. F. Baes, J. Solution Chem. **3**, 191 (1974)

10.	B. F. Hitch and R. E. Mesmer, J. Solution Chem. **5**, 667 (1976)

11.	W. L. Marshall, R. Slusher, and E. V. Jones, J. Chem. Eng. Data **9**, 187 (1964)

12.	W. L. Marshall and E. V. Jones, J. Phys. Chem. **20**, 4028 (1966)

13.	D. D. Wagman, W. H. Evans, V. B. Parker, R. H. Schumm, I. Halow, S. M. Bailey, K. L. Churney, and R. L. Nuttall, J. Phys. Chem. Ref. Data **11**, Suppl. 2 (1982)

14.	D. L. Marquardt, J. Soc. Ind. Appl. Math. **2**, 431 (1963)

15.	R. E. Mesmer, W. L. Marshall, D. A. Palmer, J. M. Simonson, and H. F. Holmes, J. Solution Chem. **21**, 699 (1988)

16.	S. V. Mattigod, D. Rai, A. R. Felmy and L. Rao, J. Solution Chem. **26**, 391 (1997)

17.	J. W. Larson, P. Cerutti, H. K. Garber, and L. G. Helper, J. Phys. Chem. **72**, 2902 (1968)

18.	J. R. Fisher and E. Zen, Amer. J. Sci. **270**, 297 (1971)

19.	G. T. Bhandage, J. A. K. Tareen and B. Basavalingu, J. Thermal Anal. **32**, 1823 (1987)

20.	P. Pan and A. B. Campbell, J. Solution Chem. **26**, 461 (1997)

21.	M. Yasuda, K. Fukumoto, Y. Ogata and F. Hine, J. Electrochem. Soc. **135**, 2982 (1988)

22. V. P. Vasil'ev and V. A. Borodin, Russ. J. Inorg. Chem. **32**, 1099 (1987)

23. I. Barin, *Thermochemical Data of Pure Substances*, (VCH Verlagsgesellschaft, Weinheim, 1989)

24. M. H. Abraham and Y. Marcus, *J. Chem. Soc. Faraday Trans. I,* **82**, 3255 (1986)

25. C. M. Criss and J. W. Cobble, *J. Amer. Chem. Soc.* **86**, 5390 (1964)

LIST OF TABLES

Table I

Feedwater Compositions

Run	Ammonia mmol kg^{-1}	pH at 25°C	Conductivity μS cm^{-1}
1	0.074	9.35	7.8
1 (old)*	0.075±0.029	9.39±0.04	7.44±0.19
1A/B	0.074	9.35	7.2
2	0.710	9.90	27.5
2A/B	0.737	10.05	28.3
3	5.70	10.40	83.8
3A	5.70	10.53	83.7
	NaOH mmol kg^{-1}		
4	0.19	10.33	47.8
4A	0.17	10.26	44.0
5	2.33	11.37	579
5A	2.05	11.31	510
6A	3.91	11.58	951

* Data taken during Ref. (2) test program; P = 9.31 MPa.

Table II

Solubilities of NiO/Ni(OH)$_2$ in Aqueous Solutions*

Ni**	T (K)	Ni**	T (K)	Ni**	T (K)	Ni**	T (K)	Ni**	T (K)
Run 1		Run 1 (old)		Run 2		Run 3		Run 4	
106.	294.8	112.	296.5	47.7	296.5	59.6	296.5	30.0	295.4
182.	313.7	245.	326.5	51.1	313.2	40.9	311.5	28.4	312.0
257.	324.3	271.	342.6	44.3	324.8	37.5	324.8	21.3	324.3
232.	338.2	347.	355.4	51.1	338.7	29.0	338.7	19.9	338.7
325.	350.4	409.	367.0	49.4	350.9	22.1	351.5	12.9	350.9
376.	362.0	376.	382.6	49.4	363.2	12.4	366.5	13.8	352.6
424.	382.6	453.	394.8	47.7	380.4	11.4	380.9	11.6	365.4
416.	395.4	419.	408.2	47.7	394.3	10.6	394.3	9.9	380.9
395.	408.7			42.6	408.2	10.6	408.2	9.0	394.3
371.	408.2			40.9	422.0	9.5	422.0	8.3	410.9
								8.2	422.0
Run 1A		Run 1B		Run 2A		Run 2B		Run 3A	
436.	422.0	365.	422.0						
368.	435.9	286.	435.9	(112)	435.9	35.6	435.9	9.4	435.9
276.	449.8	245.	449.8	33.0	449.8	32.5	449.8	8.7	449.8
216.	463.2	186.	463.7	(47.2)	463.7	27.6	463.7	8.0	463.2
181.	477.6	143.	477.6	23.0	477.6	22.5	477.6	7.0	477.6
124.	491.5	101.	491.5	(35.3)	491.5	15.2	491.5	7.2	491.5
86.9	504.8	64.6	504.8	(21.5)	505.4	14.0	505.4	8.0	504.8
46.8	518.7	56.7	519.3	17.4	519.3	9.2	519.3	8.2	518.7
30.7	533.2	40.7	533.7	11.4	533.7	10.0	533.2	7.5	533.2
36.8	547.0	32.7	546.5	11.1	546.5	11.6	547.6	6.6	547.0
28.1	560.9	31.2	560.9	9.4	560.9	11.1	560.4	6.8	560.9
22.7	575.4	26.9	574.3	10.4	574.8	10.0	574.8	6.8	574.8
22.7	588.7	(34.1)	588.7	9.5	588.7	11.6	588.7	8.9	588.7

*   All concentrations determined by GFAA except for Run 1 (old). Parentheses denote suspect data exhibiting hysteresis that were excluded from least-squares analysis.

**   Units: 10^{-9} mol-kg water^{-1}.

Table III

Measured Solubilities of Bunsenite (NiO)*

Ni**	T(K)	Ni**	T(K)	Ni**	T(K)	Ni**	T(K)	Ni**	T(K)
Run 5		Run 3B		Run 4A		Run 5A		Run 6A	
1.5	295.9	10.3	435.9	6.73	435.9	0.65	435.9		
1.6	312.0	9.47	449.8	5.25	450.9	0.49	449.8		
1.7	324.8	8.94	463.2	4.45	463.7	0.46	463.7		
1.7	339.8	7.89	477.6	3.49	478.7	0.49	477.6	0.63	477.6
1.4	350.9	8.35	491.5	3.00	491.5	0.49	491.5	0.65	491.5
1.4	365.4	7.19	504.8	2.35	505.4	0.53	505.4	0.56	505.4
1.0	380.9	6.32	518.7	1.96	519.3	0.58	519.3	0.60	519.3
0.9	394.3	6.35	533.2	2.15	533.2	0.61	533.2	0.44	533.7
		5.23	547.0	1.64	547.0	0.63	547.0	0.63	547.6
		5.52	560.9	1.26	560.9	0.58	560.9	0.70	560.9
		6.61	574.8	1.16	574.8	0.68	575.4	0.82	574.8
		6.29	588.7	1.31	588.7	0.82	588.7	1.06	588.7

* All concentrations determined by ICP-MS except Run 5 (GFAA). Duplicate sample analyses from Run 3A (GFAA), as represented by Run 3B (ICP-MS), were averaged prior to least-squares analysis.

**Units = 10^{-9} mol-kg water^{-1}

Table IV

Ionization Behavior of Selected Compounds

Compound Undergoing Ionization	b_1	b_2	b_3	b_4	b_5	Reference Cited
H_2O	31,286.0	-606.522	94.9734	-0.097611	-2,170,870	Sweeton, Mesmer and Baes [9]
NH_4OH	27,496.7	-513.761	81.2824	-0.0905795	-1,717,720	Hitch and Mesmer [10]

Table V

Thermodynamic Parameters Fitted for the Calculation of
Nickel Oxide Solubility Behavior in Sodium and Ammonium Hydroxide Solutions*

Reaction	$\Delta H°(298)$, kJ mol^{-1}	$\Delta S°(298)$, J mol^{-1} K^{-1}	$\Delta G°(298)$, kJ mol^{-1}
Dissolution			
$\beta\text{-}Ni(OH)_2(s) + 2H^+(aq) = Ni^{2+}(aq) + 2H_2O$	-89.10 ± 1.82	-72.76 ± 4.68	-67.41 ± 0.47
$NiO(s, rhombohedral) + 2H^+(aq) = Ni^{2+}(aq) + H_2O$	-98.95 ± 2.64	-96.04 ± 5.61	-70.32 ± 0.98
$NiO(s, cubic) + 2H^+(aq) = Ni^{2+}(aq) + H_2O$	**	**	(-65.84)**
Hydrolysis			
$Ni^{2+}(aq) + H_2O = Ni(OH)^+(aq) + H^+(aq)$	37.43 ± 2.24	-55.21 ± 5.74	53.89 ± 0.65
$Ni^{2+}(aq) + 2H_2O = Ni(OH)_2(aq) + 2H^+(aq)$	112.46 ± 7.05	-56.83 ± 13.22	129.41 ± 3.16
Amminocomplexing			
$Ni^{2+}(aq) + NH_3(aq) = Ni(NH_3)^{2+}(aq)$	-15.23***	0.84***	-15.48***
$Ni^{2+}(aq) + 2NH_3(aq) = Ni(NH_3)_2^{2+}(aq)$	-30.50***	-8.70***	-27.91***
$Ni(OH)^+(aq) + NH_3(aq) = Ni(OH)(NH_3)^+(aq)$	-33.30 ± 9.75	-53.54 ± 32.16	-17.34 ± 0.61
$Ni(OH)_2(aq) + NH_3(aq) = Ni(OH)_2(NH_3)(aq)$	4.28±12.17	67.07 ± 22.11	-15.72 ± 5.28

* $\ln K = -\Delta G°/RT$, where $\Delta G° = \Delta H° - T\Delta S°$

** $\Delta G°(T) = -104007 + 355.92\ T - 40\ T \ln T$. Fit constrained to give $\Delta C_p^o = 40$ J mol^{-1}K^{-1} and same $\Delta G°(520)$ as calculated for rhombohedral NiO dissolution reaction.

***   Value fixed per Ref. (22)

Table VI

Thermochemical Properties for Species in the NiO-H$_2$O System

Species	C_p^o (298)	S^o (298)	ΔH_f^o (298)	ΔG_f^o (298)	Ref.
Ni(s)	26.07	29.87	0	0	23
$-Ni(OH)_2$(s)	-	84.53	-534.98	-451.15	b
NiO(s)	44.49	37.99	-239.3	-211.1	3
H$_2$(g)	28.84	130.68	0	0	23
O$_2$(g)	29.38	205.15	0	0	23
H$_2$O(aq)	75.29	69.95	-285.83	-237.14	23
H$^+$(aq)	-71.	-22.2	0	0	24, 25
Ni^{2+}(aq)	-191.6	-172.5	-52.42	-44.28	b, 20
Ni(OH)$^+$(aq)	-	-135.6	-300.82	-227.53	b
Ni(OH)$_2$(aq)	-	-45.1	-511.62	-389.15	b
Ni(OH)$_3^-$(aq)	-	-100.8	-793.07	-577.82	2

[a] Units: C_p^o, J mol^{-1} K^{-1}; S^o, J mol^{-1} K^{-1}; ΔH_f^o, ΔG_f^o, kJ mol^{-1}.

[b] This work; bunsenite solubility calculations above 246°C should allow for a loss of magnetic ordering (see Table V).

LIST OF FIGURE CAPTIONS

Fig. 1. Comparison of higher angle X-ray diffraction peaks for coarsened NiO with lines for rhombohedral (**C**) and cubic (----) nickel(II) oxide; copper K$_\alpha$ radiation).

Fig. 2. Schematic of flowing autoclave system used in nickel oxide solubility investigation.

Fig. 3. High magnification SEM photographs of nickel(II) oxide surface before (upper) and after (lower) solubility testing (3,000 - 10,000X).

Fig. 4. Oxygen (1s) X-ray photoelectron spectra of nickel(II) oxide surface: (a) pretest and (b) posttest; both after Ar sputtering for 12 s to remove carbon surface contamination. The solid line drawn through the data represents the sum of the individual band fits within the envelope. Note the appearance of a hydrous Ni(II) oxide surface phase (OH$^-$ bond at 531.4 eV) upon exposure to the aqueous environment.

Fig. 5. Comparison of measured and predicted solubilities of (hydrous) nickel(II) oxide in aqueous ammonium hydroxide: Runs 1/1A/1B, NH$_3$ $_\cdot$ 0.07 mmol kg^{-1} ; Runs 2/2A/2B, NH$_3$ $_\cdot$ 0.7 mmol kg^{-1}.

Fig. 6. Comparison of measured and predicted solubilities of (hydrous) nickel(II) oxide in aqueous sodium hydroxide: Runs 4/4A, NaOH $_\cdot$ 0.19 mmol kg^{-1}; Runs 5/5A, NaOH $_\cdot$ 2. mmol kg^{-1}.

Fig. 7. Comparison of measured and predicted solubilities of (hydrous) nickel(II) oxide in alkaline solutions: Runs 3/3A/3B, NH$_3$ $_\cdot$ 7 mmol kg^{-1}; Run 6, NaOH $_\cdot$ 4 mmol kg^{-1}.

Fig. 8. Free energy changes for theophrastite/bunsenite dissolution reactions in aqueous solutions. Eqs. (14, 15) predictions shown as dashed lines.

Fig. 9. Free energy changes for first two hydrolysis reactions of the Ni(II) ion.

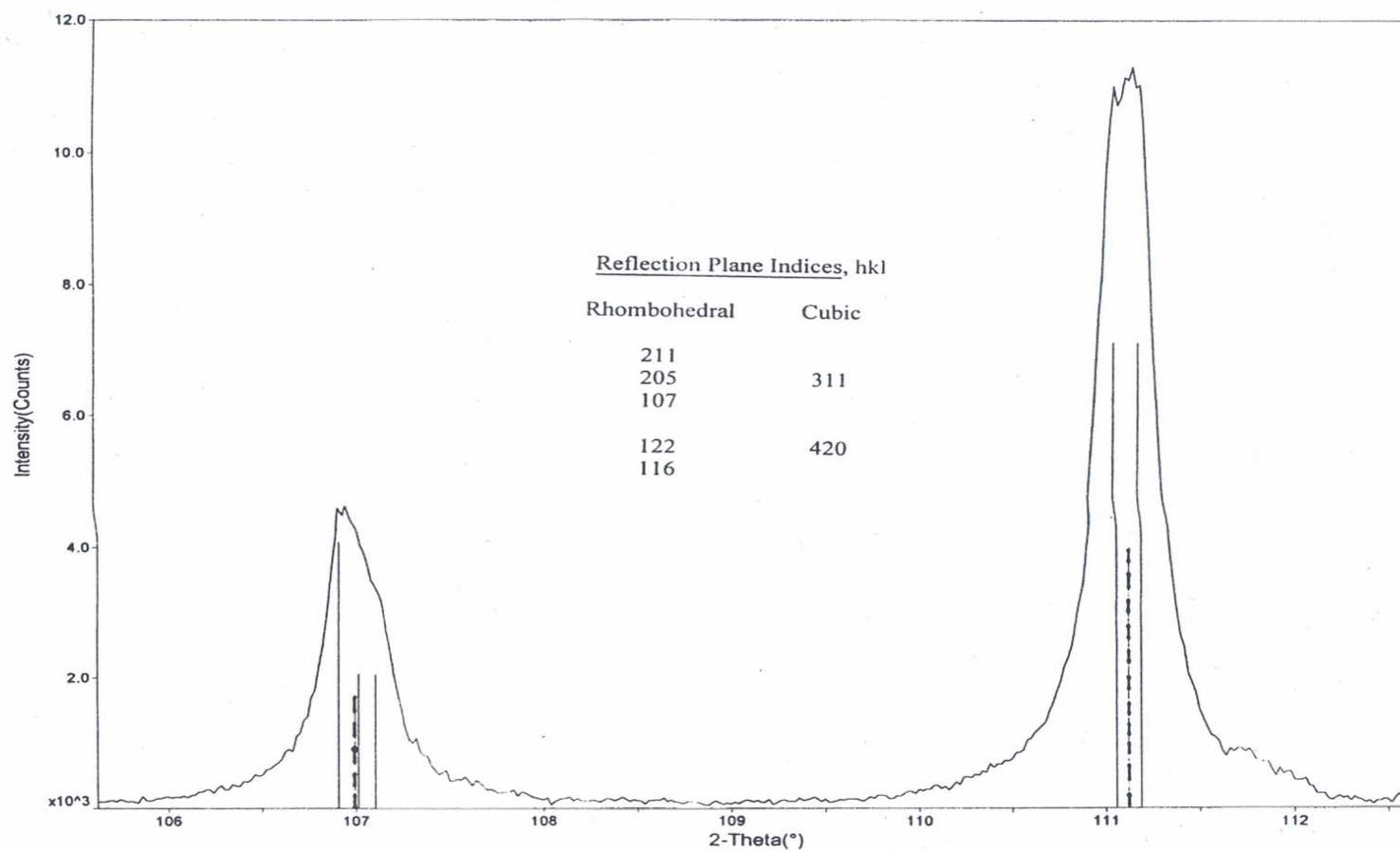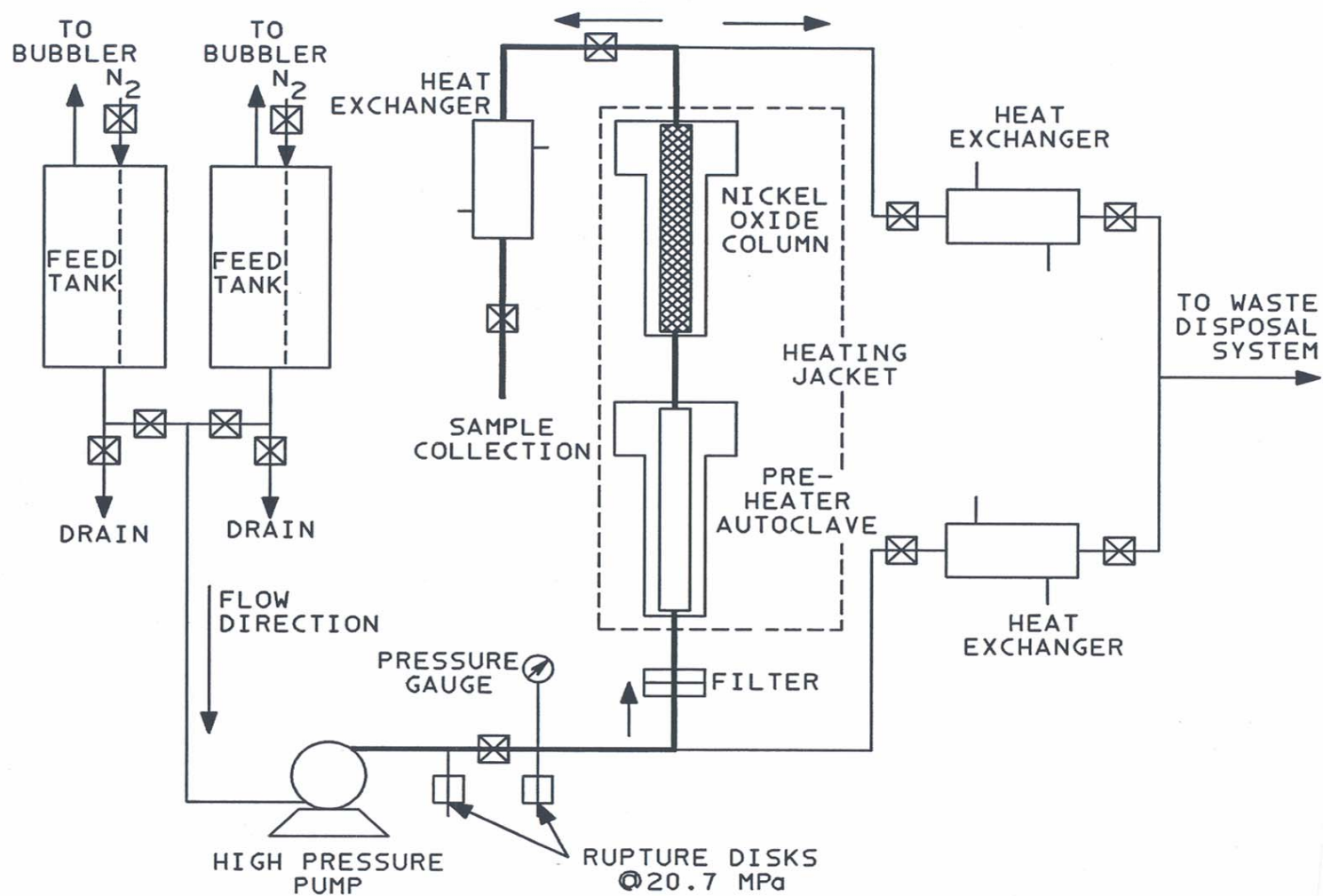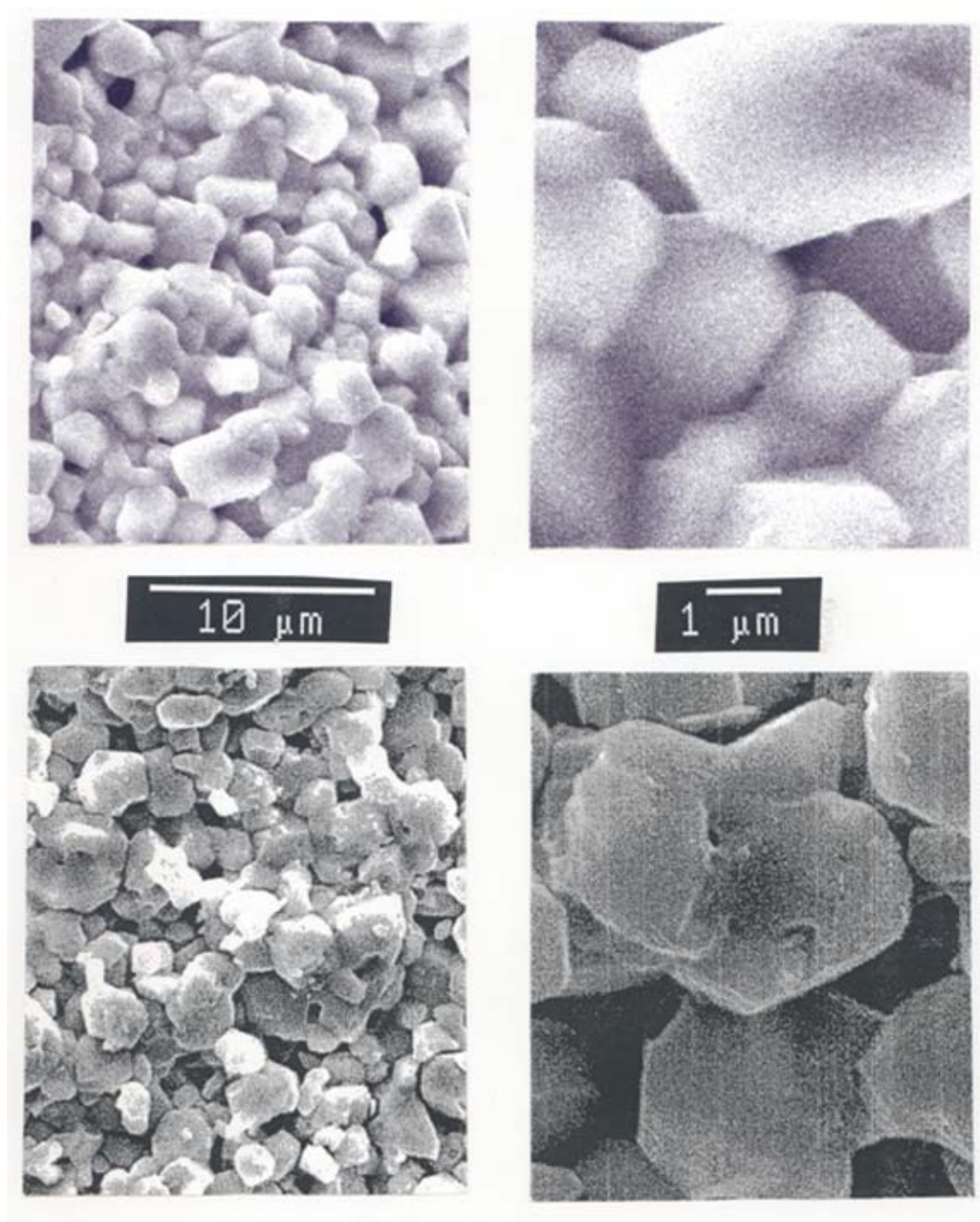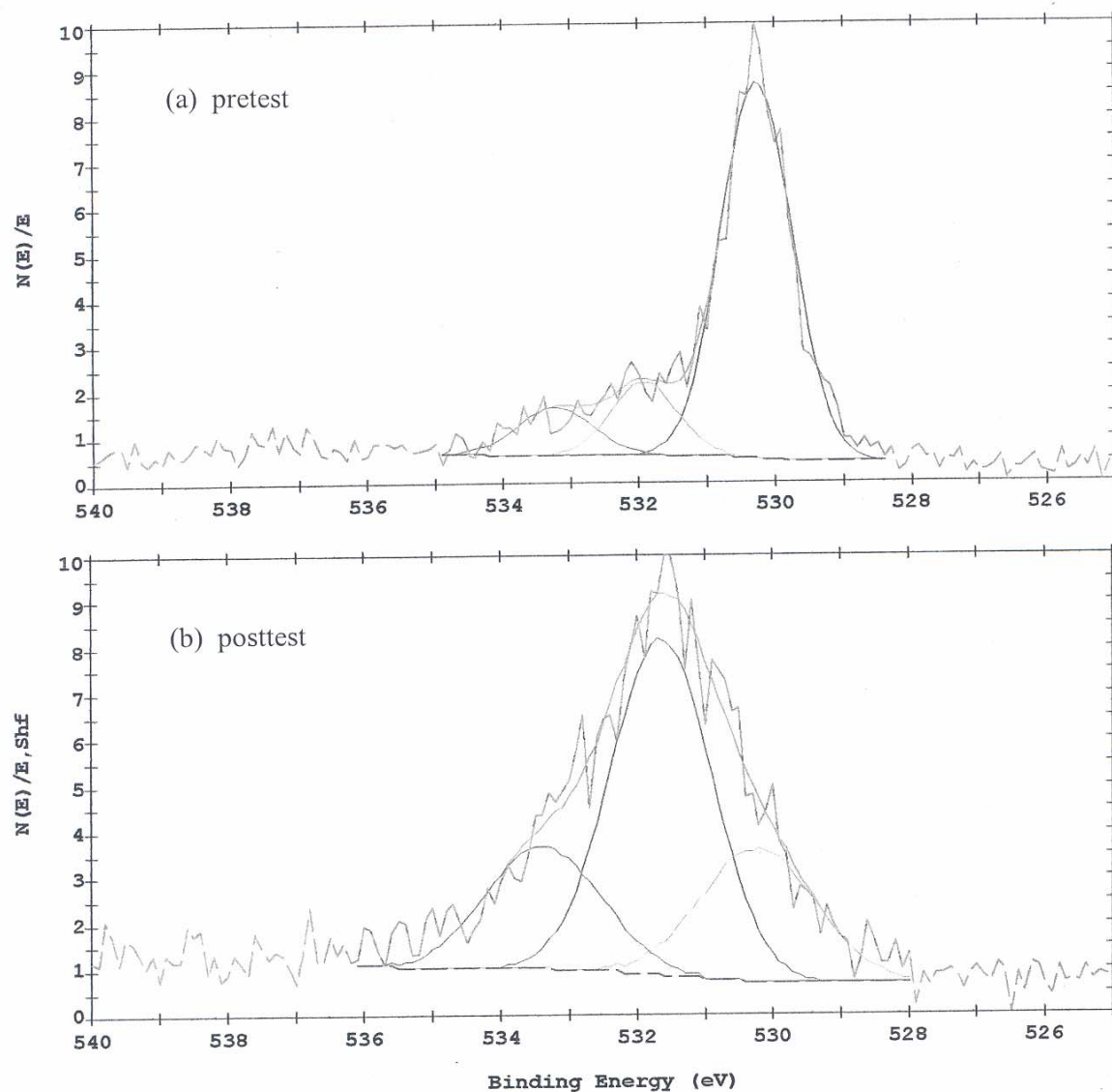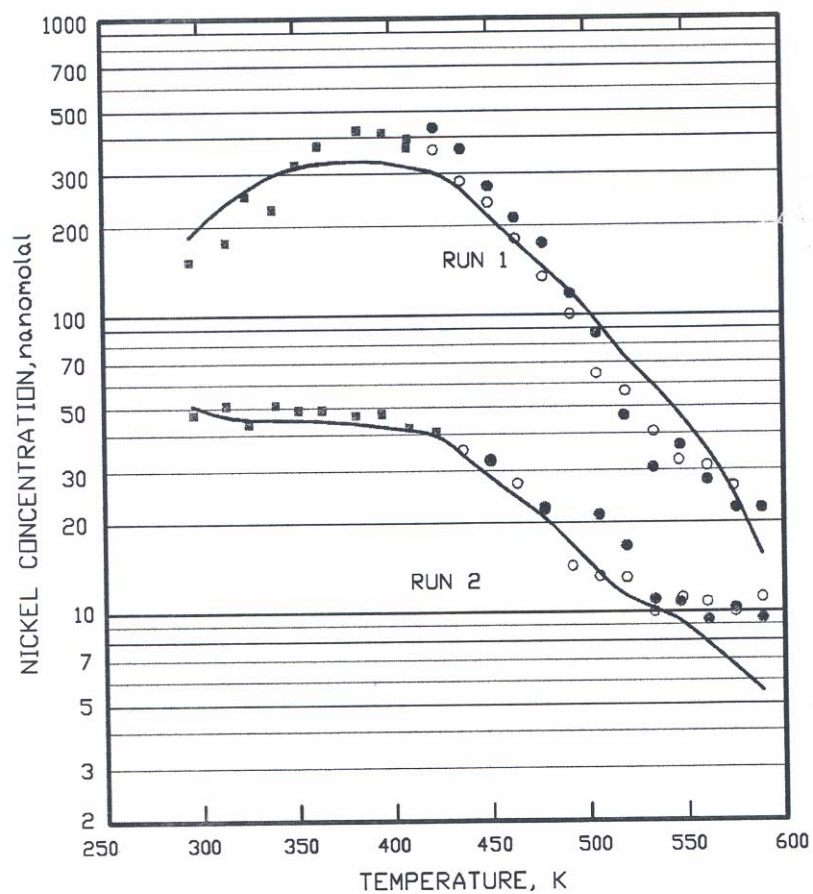Fig. 10.Free energy changes for amminocomplexing reactions of Ni(II) ion hydrolysis products.

Fig. 1. Comparison of higher angle X-ray diffraction peaks for coarsened NiO with lines for rhombohedral (**C**) and cubic (----) nickel(II) oxide; copper K_α radiation).

Fig. 2. Schematic of flowing autoclave system used in nickel oxide solubility investigation

Fig. 3. High magnification SEM photographs of nickel(II) oxide surface before (upper) and after (lower) solubility testing (3,000 - 10,000X).

Fig. 4. Oxygen (1s) X-ray photoelectron spectra of nickel(II) oxide surface: (a) pretest and (b) posttest; both after Ar sputtering for 12 s to remove carbon surface contamination. The solid line drawn through the data represents the sum of the individual band fits within the envelope. Note the appearance of a hydrous Ni(II) oxide surface phase (OH⁻ bond at 531.4 eV) upon exposure to the aqueous environment.

Fig. 5. Comparison of measured and predicted solubilities of (hydrous) nickel(II) oxide in aqueous ammonium hydroxide: Runs 1/1A/1B, NH_3 0.07 mmol kg^{-1} ; Runs 2/2A/2B, NH_3 0.7 mmol kg^{-1}.

Fig. 6. Comparison of measured and predicted solubilities of (hydrous) nickel(II) oxide in aqueous sodium hydroxide: Runs 4/4A, NaOH ₌ 0.19 mmol kg^{-1}; Runs 5/5A, NaOH ₌ 2. mmol kg^{-1}.
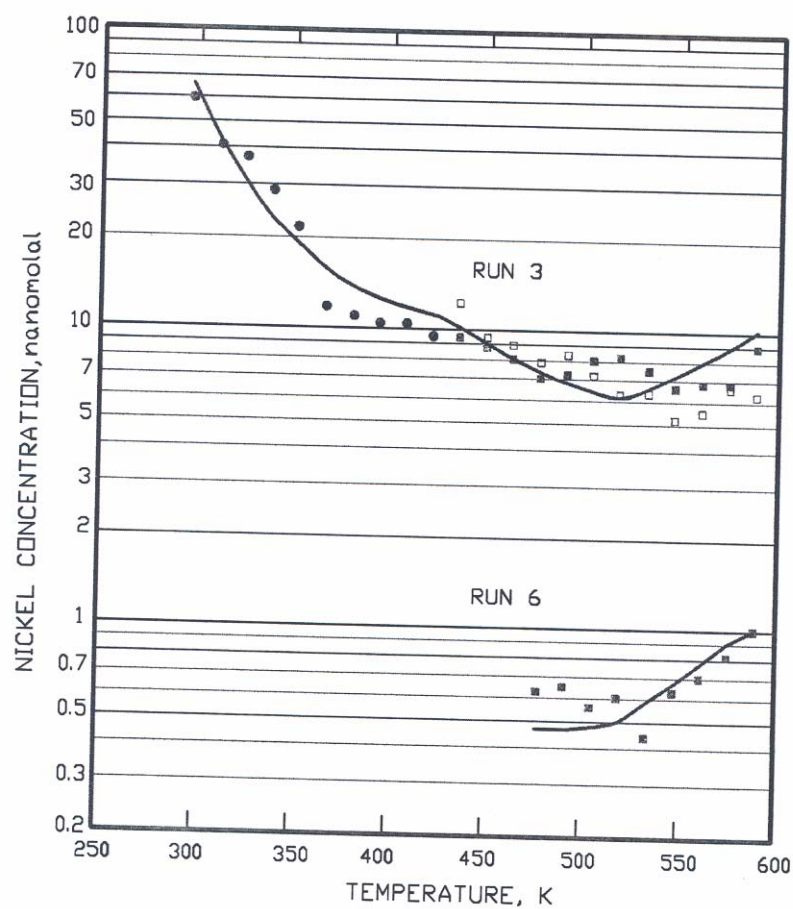
Fig. 7. Comparison of measured and predicted solubilities of (hydrous) nickel(II) oxide in alkaline solutions: Runs 3/3A/3B, NH_3 . 7 mmol kg^{-1}; Run 6, NaOH . 4 mmol kg^{-1}.
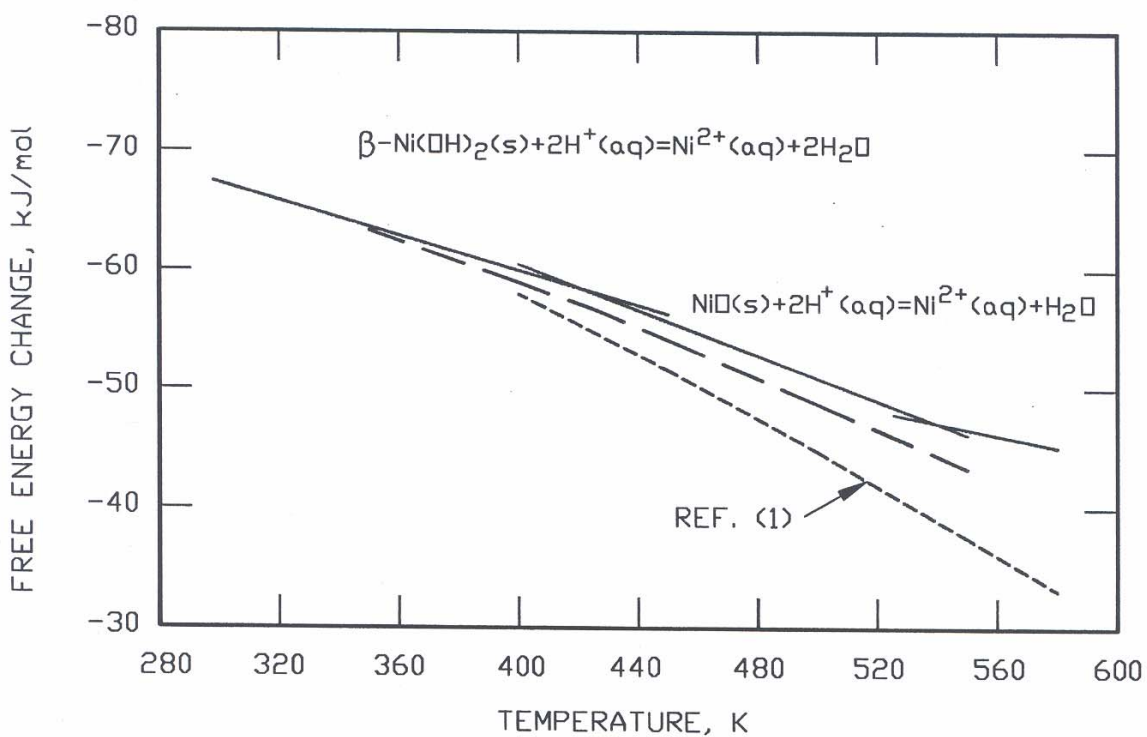
Fig. 8. Free energy changes for theophrastite/bunsenite dissolution reactions in aqueous solutions. Eqs. (14, 15) predictions shown as dashed lines.
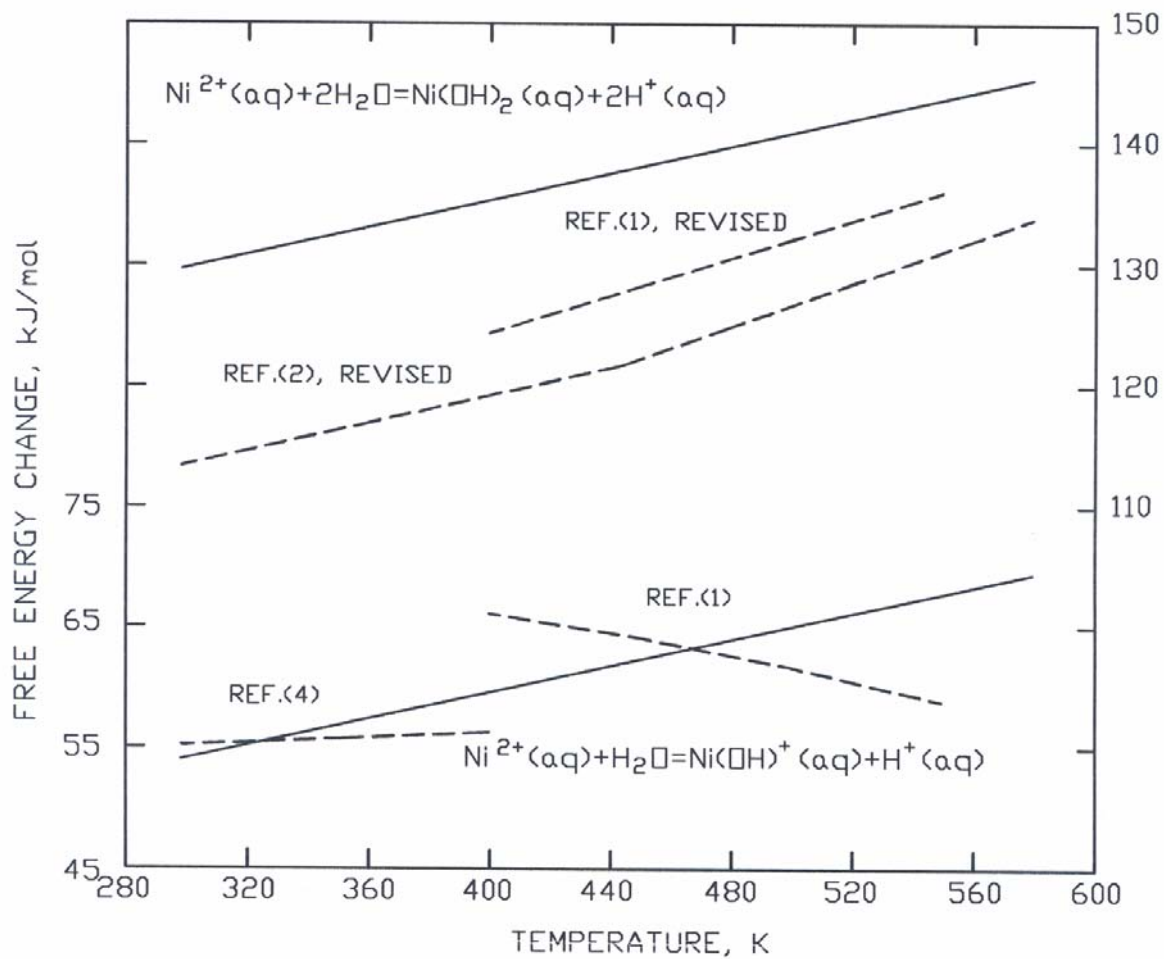
Fig. 9. Free energy changes for first two hydrolysis reactions of the Ni(II) ion.
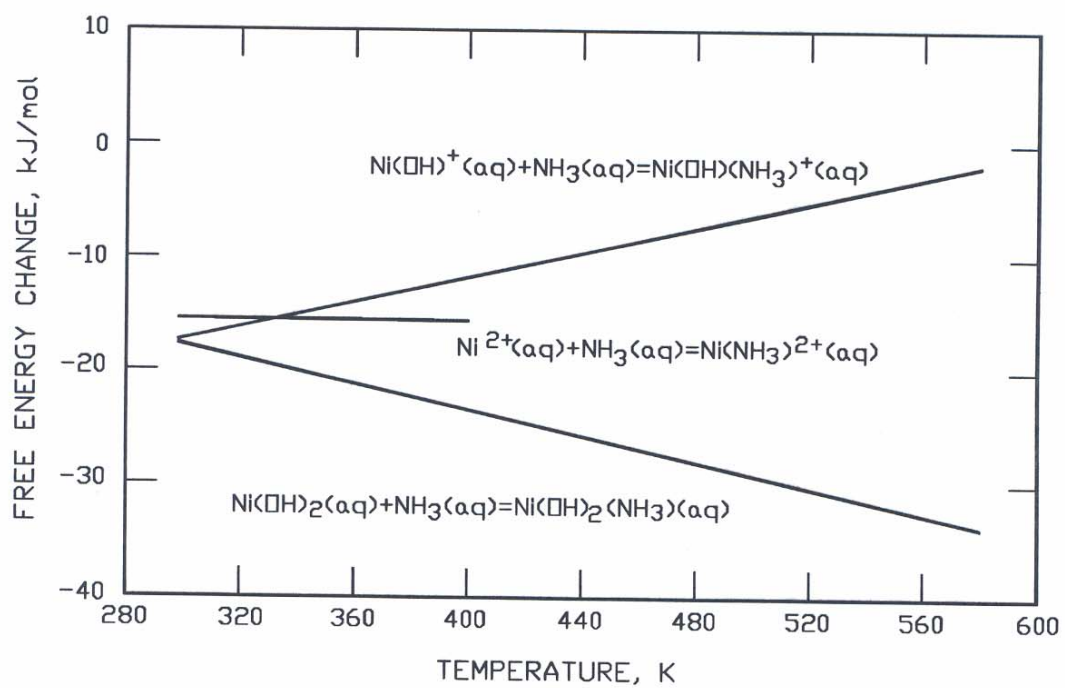
Fig. 10.   Free energy changes for amminocomplexing reactions of Ni(II) ion hydrolysis products.